IEEE Access
Multidisciplinary ⋮ Rapid Review ⋮ Open Access Journal

Received 27 November 2023, accepted 5 December 2023, date of publication 7 December 2023,
date of current version 13 December 2023.

Digital Object Identifier 10.1109/ACCESS.2023.3340706

RESEARCH ARTICLE

Transient Stability Analysis and Enhancement of PLL-VSC Considering State-Dependent Damping

DENGKE XU AND MENG ZHAN, (Senior Member, IEEE)
State Key Laboratory of Advanced Electromagnetic Engineering and Technology, School of Electrical and Electronic Engineering, Huazhong University of Science and Technology, Wuhan 430074, China

Corresponding author: Meng Zhan (zhanmeng@hust.edu.cn)

This work was supported by the National Natural Science Foundation of China under Grant U22B6008 and Grant 12075091.

ABSTRACT As a typical power electronics interface device, the voltage source converter (VSC) usually uses phase-locked loop (PLL) to synchronize with the grid and its transient synchronous dynamics is complicated. Recently it is found that the PLL-VSC system can be described by a generalized swing equation which is similar to the swing equation for the synchronous generator. Differently it has a state-dependent damping term and the basin boundary of the stable operating point can show either a closed-loop or a fish-like pattern under different parameters. To deal with these difficulties, a trajectory reversing method is proposed to efficiently obtain the basin boundary of the post-fault stable operating point, and further the critical clearing angle and the associated critical clearing time. In addition, for the transient stability enhancement, an adaptive control strategy by varying equivalent PI controller parameters of PLL in terms of the system status is proposed. It is found that it can efficiently and quickly damp transient disturbances. Therefore, these two novel methods including the trajectory reversing method and the adaptive control method are expected to be valuable for transient stability analysis and enhancement of the PLL-VSC system.

INDEX TERMS Voltage source converter, transient stability analysis, transient stability enhancement, state-dependent damping, trajectory reversing method, adaptive control.

I. INTRODUCTION

Nowadays, with the fast development and integration of various power electronic and renewable energies devices, the modern power system are facing some fundamental challenges [1], [2], [3], [4], [5]. For the power electronic devices, the control strategies are usually diverse and the control loops are complicated featured with a clear multi-time-scale character [6]. The equivalent inertia for the power electronic devices is believed as decreasing, compared to that of synchronous generator (SG) in the traditional power systems, and some methods such as virtual inertia and frequency support were proposed to deal with this tough problem recently [7]. Due to the much complicated multi-scale nonlinear dynamical behavior, this tendency also makes the transient stability analysis, assessment, and enhancement of the new-generation power system exceedingly difficult [6].

The associate editor coordinating the review of this manuscript and approving it for publication was Feiqi Deng.

As a typical power electronics interface device, the voltage source converter (VSC) usually uses phase-locked loop (PLL) to synchronize with the grid [8]. In a contrast to this grid-following method, there is another category, i.e., the so-called grid-forming method, such as power synchronization control, droop, droop with low-pass filter, and virtual synchronization generator (VSG) etc. In this paper, the PLL-based VSC system is mainly studied. For the transient stability analysis, several methods including the time-domain simulation, phase portrait, equal area criterion (EAC), energy function, bifurcation analysis, etc have been developed recently [8], [9], [10], [11], [12], [13], [14], [15], [16], [17]. Although the time-domain simulation always shows the dynamic process properly and it has been broadly used to verify the accuracy of system modeling [9] and the efficiency of transient stability enhancement strategies [10], it is time-consuming and inconvenient. In [11], the phase portrait was used to evaluate the transient stability on the two-dimensional state space. The Taylor series was used to expand the nonlinear

functions about the angle and time during the fault stage [12]. By ignoring the damping term completely, the classical EAC can give qualitative results for some faults [13]. In [14], an improved equal area criterion was proposed to improve the accuracy by considering the nonlinear damping and study how the parameters influence the transient stability. In [15] and [16], the Lyapunov's direct method was used to estimate the region of attraction. However, this method is difficult to be understood from the physical perspective. In [17], the sum-of-squares programming technique was used to improve the accuracy of the stability region by considering the indefinite damping effect, but it was still conservative.

In addition, a (normalized) generalized swing equation for the PLL-based VSC system was proposed by us [13], showing a similarity to the swing equation for the SG with a sole difference: the state-dependent damping term [13], [18]. By the bifurcation analysis, it shows that there are three different kinds of bifurcations including saddle-node, Hopf, and homoclinic bifurcations. Within the different parameter regions, the basin boundary of the stable operating point can be either a closed-loop pattern (surrounded by an unstable limit cycle) or a fish-like pattern. Therefore, the state-dependent damping effect in the generalized swing equation may bring an essential difficulty in the transient stability analysis, as there still lacks an efficient analytical method to deal with it.

For the nonlinear analysis of the PLL-VSC system, bifurcations under different parameters and models were studied [2], [19], [20]. However, the discrimination of homoclinic bifurcation is usually difficult, and a simple criteria of homoclinic bifurcation is needed. A method will be given in the later chapter based on the trajectory reversing method. And two kinds of stability regions can be observed clearly, which proves that limit cycle exists in VSC.

On the other hand, for the transient stability enhancement of the PLL-VSC systems, several control strategies have already been proposed. Generally they can be classified into two categories [18]. The first one is to modify the active current or active power during the fault. For example, the reactive current and active current were adjusted with different levels of voltage sag [10]. The other one is to modify the PLL parameters directly. For example, an increase of proportional gain and a decrease of integral gain were suggested [21]. In [22], a novel method was proposed to ensure a positive damping coefficient during fault occurrence. A gain of PI output in the PLL is added to the q-axis voltage of PLL during the fault. For the parameter variation, some adaptive control strategies can be used. For instance, a fuzzy controller was used to replace the PI controller of the PLL and make the transient response faster [23]. In [24], it was suggested that the best controller parameters are calculated online and recorded in a parameter table for different fault types and different levels of voltage dip, and the controller parameters are changed dynamically based on the parameter table when a real fault happens. To the best knowledge of the authors, as the VSC is highly controllable, there is still much open space for developing new control strategy, which should be not only easily understandable but also efficiently applicable.

To deal with the above two key problems of transient stability analysis and enhancement in the PLL-based VSC system, the trajectory reversing method (TRM) is introduced, which has been widely used to estimate the asymptotic stability regions in the traditional power systems and general dynamical systems as well [25], and the adaptive control method, which was originally used in variable droop constant control for VSC-MTDC [26] and the VSG-based VSC system [27], respectively. The TRM can also be called as time reversing method. Although the state-dependent damping effect brings certain difficulties, these two methods are of model independence and capable of overcoming these difficulties easily. With the TRM, two different (closed-loop or fish-like) patterns of basin of attraction can be easily identified and further the critical clearing angle (CCA) and the critical clearing time (CCT) for the cross-section of during-fault trajectory and basin boundary can be directly obtained. It is notable that in a very recent paper, the TRM has been mentioned in the study of the fish-like pattern of the similar system [28]. However, the closed-loop pattern is not discussed in the paper. In this paper, the two kinds of stability regions are discussed together, which means homoclinic bifurcation happens when parameters change. The corresponding criteria is proved useful. On the other hand, for the adaptive control method, the PI parameters of the PLL can be easily chosen under different system statuses, based on a simple physical understanding. The adaptive PI parameters based on the equivalent damping and inertia can be used to improve transient satbility.

The rest part of this paper is structured as follows: Section II introduces the trajectory reversing method based on the system modeling of the generalized swing equation, accompanying with the verification results and comparison results with the EAC. Section III introduces the adaptive PI parameters control strategy for the transient stability enhancement. Finally, conclusions are given in Section IV.

II. TRANSIENT STABILITY ANALYSIS BASED ON TRAJECTORY REVERSING METHOD

A. TRANSIENT MODEL FOR PLL-VSC

Fig.1 shows a single-VSC-infinite-bus model, namely, a PLL-based VSC is connected to the grid. The PLL is a synchronous loop based on the grid-following control. If the VSC loses synchronization in the transient process, the frequency of PLL would deviate from the working frequency of the AC grid. Here ACC is used to denote the alternative current control. PI controller is widely used in the ACC and PLL because the input of PI controller will decay to zero gradually when the system is stable, and the input can be controlled well. In our previous work, the PI controller is used in the VSC modeling [2]. For simplicity, the AC grid has been replaced by an ideal infinite bus. U_g is the equivalent voltage of the infinite bus, and L_f is the filter inductance.

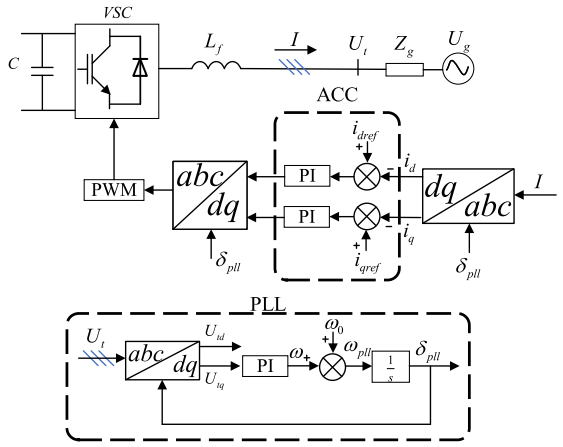

FIGURE 1. Schematic show of a VSC tied to AC grid with PLL and ACC.

Z_g=R_g+jωL_g is the equivalent grid impedance, U_t is the terminal voltage of the VSC. I_{dq}^{ref}=i_{dref}+ji_{qref} denotes the d-axis and q-axis currents in the PLL reference frame. I is the output current vector of the VSC. ω_0 is the synchronous angular frequency, and δ_{pll} and ω_{pll} are the output angle and frequency of the PLL, respectively.

As the bandwidth of the ACC is much higher than that of the PLL, the current output can be believed as always following the current references, which are set as constants in the paper. Therefore, the VSC can be treated as a controlled current source and its dynamics is determined by the PLL solely. Under this simplification, the transient dynamics of the PLL-VSC system can be expressed by the so-called generalized swing equation, which is still a second-order equation and similar to the classical swing equation of the SG [13], [29]:

$$M_{eq}\ddot{\delta} = P_m - P_e - D_{eq}(\delta)\dot{\delta} \tag{1}$$

where

$$\begin{cases} P_m = X_g i_{dref} + R_g i_{qref} \\ P_e = U_g \sin\delta \\ M_{eq} = \dfrac{1}{k_i}(1 - \dfrac{k_p X_g i_{dref}}{\omega_0}) \\ D_{eq} = \dfrac{k_p}{k_i} U_g \cos\delta - \dfrac{X_g i_{dref}}{\omega_0} \end{cases} \tag{2}$$

Here $\delta = \delta_{pll} - \omega_0 t$ denotes the angular position deviation between the PLL and the grid, $\omega = \omega_{pll} - \omega_0$ is the corresponding angular frequency deviation. k_p and k_i are the PI parameters of the PLL. P_m and P_e are the equivalent mechanical and electromagnetic powers, respectively. M_{eq} and D_{eq} are the equivalent inertia and damping, respectively. Both M_{eq} and D_{eq} are determined by the controller parameters. Here the dominant difference with the SG is that the D_{eq} in (2) is state-dependent, i.e., it changes with the angle deviation δ, whereas the damping of the SG is always a positive constant. Clearly this state-dependent nonlinear damping could bring an additional difficulty in the transient stability problems of the PLL-VSC system.

TABLE 1. System parameters.

Symbol	Item	Value(p.u.)
k_p	Proportional gain of PLL	50
R_g	Resistance of transmission line	0
X_g	Inductance of transmission line	0.5
i_{dref}	d-axis current reference	0.6
i_{qref}	q-axis current reference	-0.4
U_{gpre}	Voltage of the infinite bus before fault	0.4
$U_{gduring}$	Voltage of the infinite bus during fault	0.25
U_{gpost}	Voltage of the infinite bus after fault	0.38
i_{dref}	Decreasing	0.6

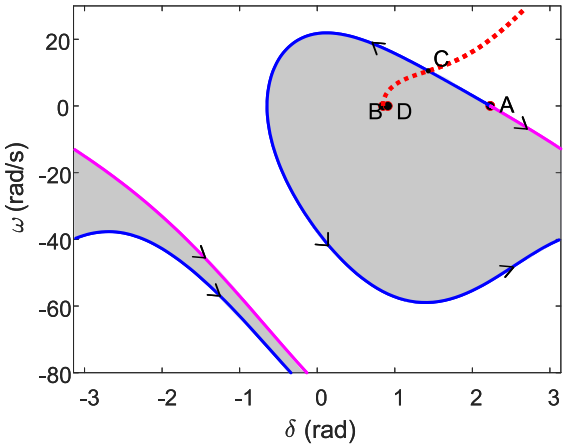

FIGURE 2. Comparison of the basin boundary (blue and pink curves) obtained by the trajectory reversing method and the basin of attraction (gray area) of the post-fault stable equilibrium point obtained by the Monte Carlo method; k_i = 1500. The dot A (D) denotes the unstable (stable) equilibrium point of the post-fault state, the dot B the stable equilibrium point of the pre-fault state, and the point C the cross-point of the basin boundary and the during-fault forward trajectory.

The equilibrium points in (1) can be easily obtained:

$$\begin{cases} \delta_s = \arcsin\dfrac{X_g i_{dref} + R_g i_{qref}}{U_g} \\ \delta_u = \pi - \delta_s = \pi - \arcsin\dfrac{X_g i_{dref} + R_g i_{qref}}{U_g} \end{cases} \tag{3}$$

where δ_s (δ_u) denotes the stable (unstable) equilibrium point. If the voltage is too small, the equilibrium point does not exist. However, usually the equilibrium point exists for the before-fault and clearing-fault states.

Ref. [13] proposed a normalized generalized swing equation to simplify the system analysis. It has been found that due to the homoclinic bifurcation, the asymptotic stability regions can be either a fish-like or an elliptic pattern. These two different types of basin have been calculated by using the Monte Carlo method by exhaustively searching all initial conditions. For each initial condition, the system may asymptotically approach to the equilibrium point or infinite after a long transient time. The initial conditions going to the equilibrium point are kept and plotted. The basins of attraction of the post-fault equilibrium point are shown by gray areas in Fig.2 and Fig.3, respectively. The only difference is the different values of k_i, namely, k_i = 1500 in Fig.2 and k_i = 10000 in Fig.3. The other system parameters are the same, as shown in Tab.1.

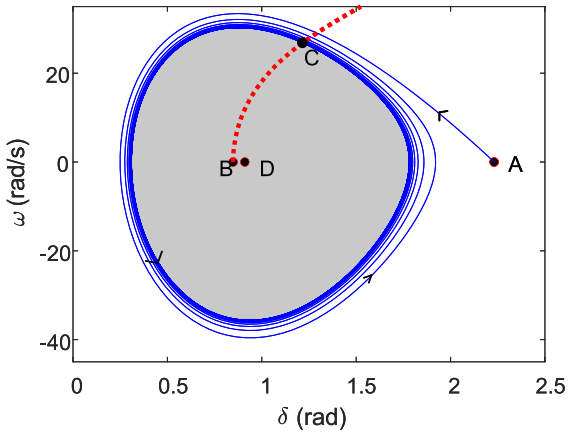

FIGURE 3. Similar to FIGURE 2, but for $k_i = 10000$ instead.

The subscripts "pre", "during", and "post" are used to denote the three fault stages in the transient process: pre-fault, during-fault, and post-fault stages, respectively. The parameters are selected just like our previous work [13], and the units of them are p.u.

In addition, the dot A (D) is used to denote the unstable (stable) equilibrium point of the post-fault state, the dot B the stable equilibrium point of the pre-fault state, and the point C the cross-point of the basin boundary and the during-fault forward trajectory.

As it is well known that the transient stability should be determined by whether the fault-clearing state is within or out of the basin of the attraction of the post-fault equilibrium point, the determination of the basin of attraction is of great importance. Different with the classical fish-like pattern in the swing equation, here not only the fish-like but also the close-form patterns should be judged for different parameters. In addition, for the close-form pattern, it is far away from the post-fault equilibrium point. All these unusual phenomena may pose a basic challenge for the transient stability analysis.

B. ALGORITHM FOR TRAJECTORY REVERSING METHOD

To solve the above troubles, the TRM is used with the associated algorithm developed. The basic idea is simple. By replacing the timing (from t to $-t$) and setting the unstable equilibrium point (UEP) of the post-fault state as the initial condition, the (reversing) trajectory from the UEP can be obtained, still by using the time-domain integration. With this method, the two different types of basin of attraction can be easily identified. Furthermore, the CCA and CCT can be easily obtained based on the intersection between the during-fault trajectory and the obtained basin boundary. It is notable that in the final step of calculation, only a small component of the basin boundary near the during-fault trajectory is needed.

In the power systems, there are many different types of faults. In this paper, without losing generality, only consider the typical voltage sag fault of the infinite bus. Based on the expressions in (2), clearly the voltage sag with the change of U_g mainly changes P_e. Therefore, the voltage sag fault is similar to the three-phase short circuit fault in the SG [13]. The UEP in the post-fault stage $\delta_{upost} = \delta_{cr}$ in (2) is critical, as the PLL-VSC will lose synchronization if δ exceeds δ_{cr} in the transient process.

With the TRM, replace t by $-t$ in (1) and obtain a new dynamic equation immediately:

$$M_{eq}\ddot{\delta} = P_m - P_e + D_{eq}(\delta)\dot{\delta} \tag{4}$$

showing the only difference of the sign of the D_{eq} term. Then start from (δ_{cr},0) and get the reverse trajectory by numerical integration. In calculation, a slight perturbation is needed. Their trajectories guided by arrows are shown in Fig. 2 for the fish-like pattern and in Fig. 3 for the close-loop pattern. In Fig. 2, it can see that with the different tiny perturbations of initial conditions (e.g., a perturbation of 10^{-10} or -10^{-10} on ω, respectively), both the top boundary (blue curve) and bottom boundary (pink curve) of the basin of attraction of the fish-type pattern can be well obtained. Whereas in Fig. 3, only the asymptotic stable limit cycle (blue curve) can be obtained. Clearly these basin boundaries obtained by the TRM (denoted by the arrows) match with the basin of attraction obtained by the Monte Carlo method (denoted by the green region) well.

After determining whether the final asymptotic behavior is a limit cycle (periodic behavior) or not, the pattern of the basin of attraction for either a close form or a fish-like one can be judged. Further, the process of estimating the boundary of the stability region is also slightly different. Firstly, to obtain the CCA, the correct part of the reverse trajectory should be chosen. When the reverse trajectory does not converge to a cycle (like Fig. 2), the initial part of the reverse trajectory will be used to obtain the cross-point with the forward during-fault trajectory, starting from (δ_0,0). Oppositely if the reverse trajectory converges to a cycle (like Fig. 3), the final limit cycle data should be used to get the cross-point. After the cross-point is obtained for these two different patterns, the corresponding CCA and CCT can be obtained immediately. A flow chart for the detailed algorithm of the trajectory reversing method is given in Fig. 4, to summarize the process for determining the two types of stability region patterns and calculating the CCA and CCT.

C. CCA/CCT CALCULATION RESULTS BASED ON TRAJECTORY REVERSING METHOD

In Fig. 2, $k_i = 1500$. And CCA=1.4325rad and CCT=0.0950s by the TRM. To check these results, the clearing time is set as 0.0950s and 0.0951s separately and calculate their corresponding time-domain responses of angle δ. The results are shown in Fig. 5, where clearly the system is stable (unstable) when the clearing time is smaller (larger) than the CCT in Fig. 5(a) [Fig. 5(b)]. They show that with an extremely tiny variation of the clearing time, the system dynamics can be completely different. They also show that the result based on the TRM is accurate with a sufficiently high precision.

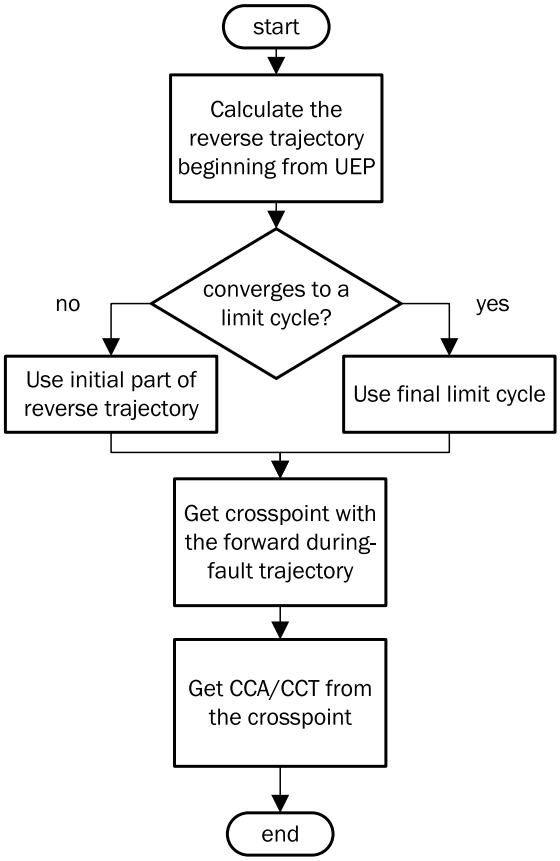

FIGURE 4. Flow chart of the algorithm of the trajectory reversing method.

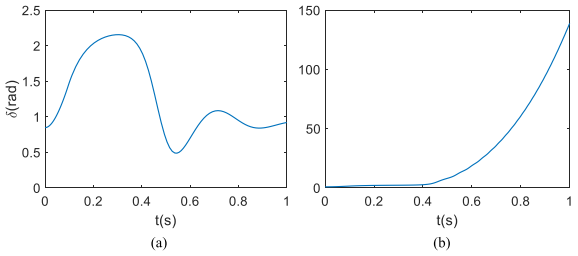

FIGURE 5. Verification of the CCT under $k_i = 1500$ by different clearing times: (a) 0.0950s and (b) 0.0951s.

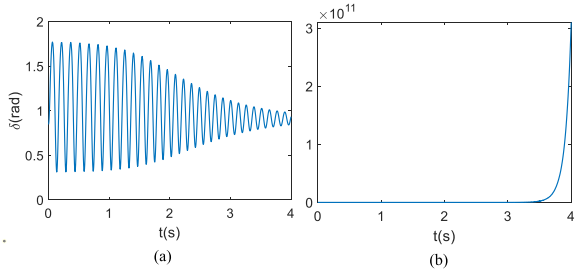

FIGURE 6. Verification of the CCT under $k_i = 10000$ by different clearing times: (a) 0.0257s and (b) 0.0258s.

Similarly, in Fig. 3 under $k_i = 10000$, CCA=1.2166rad and CCT=0.0257s from the TRM. The corresponding time-domain results are shown in Fig. 6. The clearing time is 0.0257s in Fig. 6(a) and 0.0258s in Fig. 6(b). Again the results are perfect. In addition, further study shows that with all other parameters fixed, the critical parameter for the homoclinic bifurcation is $k_i = 8407$, which is relatively very large.

All these comparisons clearly demonstrate that the TRM is efficient for the transient stability and assessment of the PLL-based VSC under different system parameters and it is workable for not only close-form but also fish-like patterns of basin of attraction. Comparatively, the calculation of the CCA is fast, compared with the Monte Carlo method. It is notable that there is no any other method to deal with these two different basins so far, to the best knowledge of the authors.

We admit that this method is relatively theoretical because the equation of the system should be known first. The trajectory is obtained based on the differential equation. Even though the accuracy has been verified in Fig. 5 and Fig. 6, the feasibility of this method should be further studied, if either the ACC effect or multiple PLL-VSC systems are considered.

D. COMPARISON WITH THE EAC RESULT

As the EAC is a classical analytical method of transient stability by neglecting the damping completely, it is interesting to make a comparison, based on the TRM. Here the CCA calculated by the TRM is denoted as CCA_{TRM}, and the CCA calculated by the EAC is denoted as CCA_{EAC}. As the TRM is highly efficient, the system parameters can be systematically studied. If $CCA_{EAC} < CCA_{TRM}$, the CCA calculated by the EAC is conservative, otherwise it is radical. In the traditional power system, as the damping is positive, the EAC is always conservative. However, here as the damping is state-dependent, which can be positive or negative, the CCA_{EAC} may be either conservative or radical. The state-dependent damping effect will be studied by the comparison of CCA_{TRM} and CCA_{EAC}.

The theoretic expression of CCA_{EAC} for the voltage sag fault is explicit [13]:

$$CCA_{EAC} = \frac{P_m(\delta_0 - \delta_{cr}) + U_{gduring}\cos\delta_0 - U_{gpost}\cos\delta_{cr}}{U_{gduring} - U_{gpost}} \tag{5}$$

To characterize the deviation, η is defined as

$$\eta = \frac{CCA_{EAC} - CCA_{TRM}}{CCA_{TRM}} \tag{6}$$

The following parameters are fixed; $k_p = 50$, $k_i = 2000$, $R_g = 0$pu, $i_{dref} = 0.8$pu, $i_{qref} = -0.2$pu, $U_{gpre} = 1$pu. The other parameters $U_{gduring}$, U_{gpost}, and X_g will be studied. In each case one parameter among them is set as a constant with the other two parameters changeable. In calculating CCA_{TRM}, both patterns of basin of attraction should be possible, as the parameter variation is relatively large.

As the first case, the contour plot of η with the variation of $U_{gduring}$ and U_{gpost} is shown in Fig. 7; $X_g = 0.5$pu is fixed. Clearly η may be positive or negative for different parameters. The line for $\eta = 0$ is nearly a horizontal straight line when $U_{gpost} \approx 0.6$pu. Generally, as U_{gpost} increases,

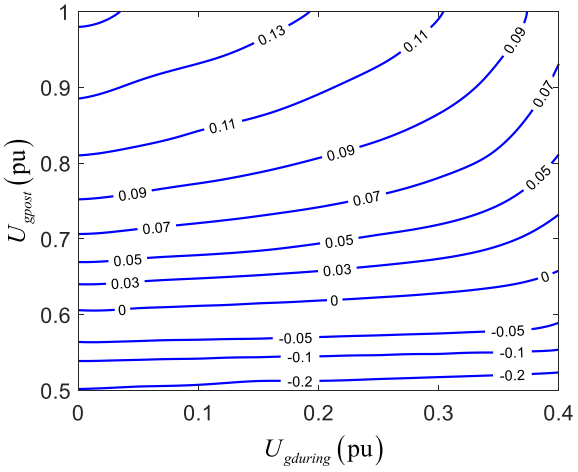

FIGURE 7. Contour plot of η with variation of $U_{gduring}$ and U_{gpost}; $X_g = 0.5$.

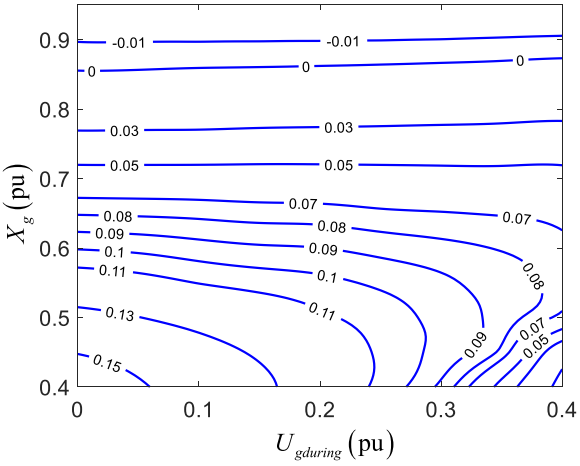

FIGURE 8. Contour plot of η with variation of $U_{gduring}$ and X_g; $U_{gpost} = 0.9$.

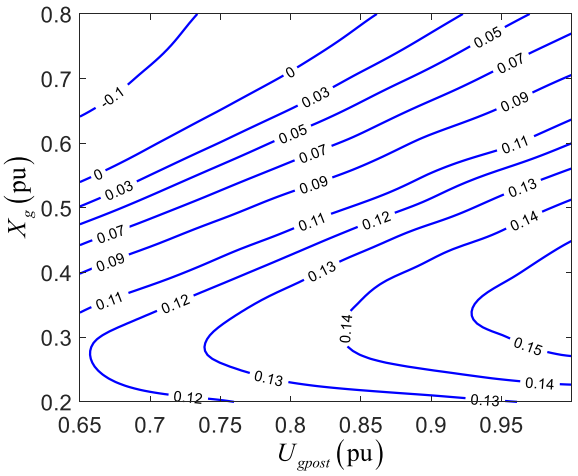

FIGURE 9. Contour plot of η with variation of U_{gpost} and X_g; $U_{gduring} = 0.1$.

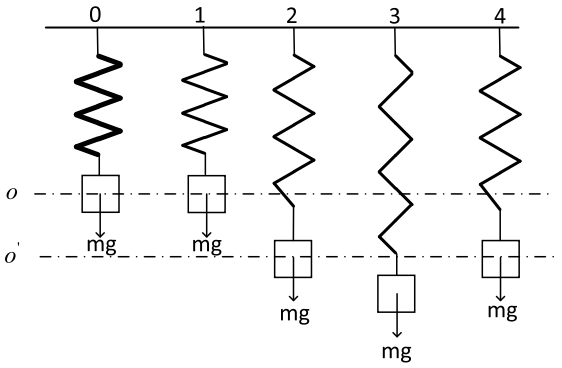

FIGURE 10. Schematic show for the transient process in the swing equation by using a mechanical equivalence. On state 0, the mass is on the pre-fault stable state *o*. In contrast, the post-fault stable state is *o'*. From states 1 to 2, it is accelerating; from states 2 to 3, it is decelerating; from states 3 to 4, it is accelerating again; and from states 4 to 1, it is decelerating. The adaptive control strategy is established by changing the (equivalent) inertia and (equivalent) damping on the basis of the system status.

η also increases. It shows that η is more likely to be influenced by U_{gpost}, compared with $U_{gduring}$.

As the second case, the contour plot of η with the variation of $U_{gduring}$ and X_g is shown in Fig. 8. $U_{gpost} = 0.9$pu. Clearly now the line for $\eta = 0$ is nearly a horizontal straight line again at $X_g \approx 0.87$pu. When X_g is relatively large, η decreases with increase of X_g and it is nearly not affected by $U_{gduring}$. When X_g is small, η increases as $U_{gduring}$ decreases. When X_g is very small, the shape of contour plot looks like a ridge.

For the third case, the contour plot of η with the variation of U_{gpost} and X_g is shown in Fig. 9. $U_{gduring} = 0.1$pu. Here the contour plot is nearly a series of parallel slant straight lines in the upper-left part of the figure. As U_{gpost} increases and X_g decreases, η increases from negative to positive. In the lower-right part, a ridge shape also occurs.

From the above figures, the EAC may cause an error which is not ignorable, and the dependence of η on the system parameters are diversified. When η is small and near zero, the contours look like several parallel straight lines. When η is large, a ridge shape may occur. In addition, η is more likely to be influenced by U_{gpost} and X_g, and relatively weaker by $U_{gduring}$. Generally, under a larger U_{gpost}, a smaller X_g, and a smaller $U_{gduring}$, η increases, meaning that the CCA_{EAC} is more likely to be radical.

III. TRANSIENT STABILITY ENHANCEMENT BASED ON ADAPTIVE CONTROL

A. THEORETICAL BASIS OF THE ADAPTIVE CONTROL

It is well known that the SG dynamics is determined by the swing equation with its intrinsic property including inertia (denoted by M) and damping (denoted by D), which are always positive and unchanged in the transient process. The VSG control imitates the SG dynamics showing the same dynamical equation, but as the VSG is fully controllable, basically its inertia M and damping D can be freely chosen. Therefore, in the transient process, the system parameters including M and D can be adaptively changed. The same idea has been reported recently [27].

To understand the adaptive control better, the transient stability process of the swing equation is explaind by using a mechanical equivalence of a mass-spring system in Fig. 10 [30].

On state 0, the mass is on the pre-fault stable state o denoted by a dashed horizontal line, due to the balance of the gravity force and the elastic force from the mechanical spring. When a large-signal disturbance happens suddenly, the gravity force becomes larger than the new elastic force. A thin spring is used to show a smaller elastic coefficient. Therefore, the motion of the mass is accelerating downward. In contrast, using o' and the dashed horizontal line to denote the post-fault stable state. Clearly from states 1 to 2, it is accelerating. However, from states 2 to 3, it is decelerating, although its speed direction is still downward. After that, from states 3 to 4, it is accelerating again, and from states 4 to 1, it is decelerating. For both states 3-4 and 4-1, the speed direction becomes upward. Based on these observations, the adaptive control strategy can be designed.

As in the transient process of the VSG, D is always positive, the value of D should be increased to make disturbance damp faster. However, for the change of value of M, in the accelerating stage, such as from states 1 to 2 and from states 3 to 4, M should increase to hinder its acceleration. On the other hand, in the decelerating stage, such as from states 2 to 3 and from states 4 to 1, M should decrease to make its decelerating process faster. Therefore, the change of M should be determined by not only the speed (ω) but also the acceleration ($d\omega/dt$). Here $\omega = \omega_{vsg} - \omega_0$. To combine these two factors, $d|\omega|/dt$ is used to uniquely determine the change of M. Hence list the adaptive inertia and damping coefficient control strategy in Tab. 2, where the fourth column is based on the combined conditions of ω and $d\omega/dt$ on the second and third columns in Tab. 2, respectively.

TABLE 2. Adaptive control strategy in VSG.

Stage	ω	$d\omega/dt$	$d\|\omega\|/dt$	D	M
1-2	>0	>0	>0	Increasing	Increasing
2-3	>0	<0	<0	Increasing	decreasing
3-4	<0	<0	>0	Increasing	Increasing
4-1	<0	>0	<0	Increasing	decreasing

As the adaptive control strategy in VSG has been proposed effective, now extend this simple strategy to the PLL-VSC system. After clearly examining the equivalent damping term D_{eq} in (2), one can find that comparatively its second constant part is small and thus only its first part ($\cos\delta$) is kept. Namely, $D_{eq}(\delta) \approx (k_p U_g \cos\delta)/k_i$. Under this assumption, k_p/k_i and $\cos\delta$ are combined to determine the damping efficient D_{eq}. When $\cos\delta > 0$,the damping is positive, which can enhance the transient stability, k_p/k_i should increse under this condition in order to make better use of positive damping. When $\cos\delta < 0$,the damping is negative, which harms the transient stability, k_p/k_i should decrese to reduce the effect of negative damping. Therefore, the control strategy for k_p/k_i on the fourth column in Tab. 3 for different δ is given.

TABLE 3. Adaptive PI parameter control strategy in PLL-VSC.

Condition	$\omega\frac{d\omega}{dt}$	$\cos\delta$	k_p/k_i	k_i
1	>0	>0	Increasing	Decreasing
2	<0	>0	Increasing	Increasing
3	>0	<0	Decreasing	Decreasing
4	<0	<0	Decreasing	Increasing

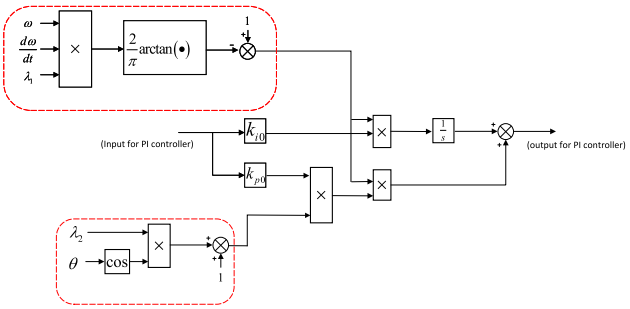

FIGURE 11. Improved adaptive PI parameter control strategy in PLL-VSC.

In addition, still relying on the generalized swing equation in (2), $M_{eq} \approx 1/k_i$. According to Tab. 2, when $\omega\frac{d\omega}{dt} > 0$, M_{eq} should increase (k_i decrease), when $\omega\frac{d\omega}{dt} < 0$, M_{eq} should decrease (k_i increase). Thus, the control strategy for k_i on the fifth column in Tab. 3 is given.

The whole control strategy for the PLL-VSC has been summarized in Tab. 3, which is obtained from the VSG adaptive control strategy. The determining conditions for how to change the control parameters k_i and k_i under the four different conditions of $d|\omega|/dt$ and $\cos\delta$ are explicit. Clearly it is easy to use. Below let us design the control strategy more explicitly.

B. SPECIFIC DESIGN PROCESS OF ADAPTIVE CONTROL IN PLL-VSC

From Tab. 3, the PI parameter of PLL should be changeable in the transient process. When $\omega\frac{d\omega}{dt} > 0$, k_i decreases, so a kind of equation of k_i can be given as

$$k_i = k_{i0}(1 - \frac{2}{\pi} arctan(\lambda_1 \omega \frac{d\omega}{dt})) \tag{7}$$

where k_{i0} denotes the initial integral parameter, and λ_1 denotes the coefficient selected to multiply with $\omega\frac{d\omega}{dt}$, which can be set relatively large. The value of tangent function is restricted within $(-\frac{\pi}{2}, \frac{\pi}{2})$. The coefficient $\frac{2}{\pi}$ can restrict $(1 - \frac{2}{\pi} arctan(\lambda_1 \omega \frac{d\omega}{dt}))$ within (0,2), so k_i is always positive, which makes M_{eq} always positive. When $\lambda_1 \omega \frac{d\omega}{dt} > 0$, $arctan(\lambda_1 \omega \frac{d\omega}{dt}) > 0$, $k_i > k_{i0}$. When $\lambda_1 \omega \frac{d\omega}{dt} < 0$, $arctan(\lambda_1 \omega \frac{d\omega}{dt}) < 0$, $k_i < k_{i0}$. So the equation (7) can be designed according to Tab. 3.

And the k_p/k_i should change with $\cos\delta$, similarly, k_p/k_i can be defined as:

$$\frac{k_p}{k_i} = \frac{k_{p0}}{k_{i0}}(1 + \lambda_2 \cos\delta) \tag{8}$$

where k_{p0} denotes the initial proportional parameter, and λ_2 denotes the coefficient that multiplied to $\cos\delta$. λ_2 should be

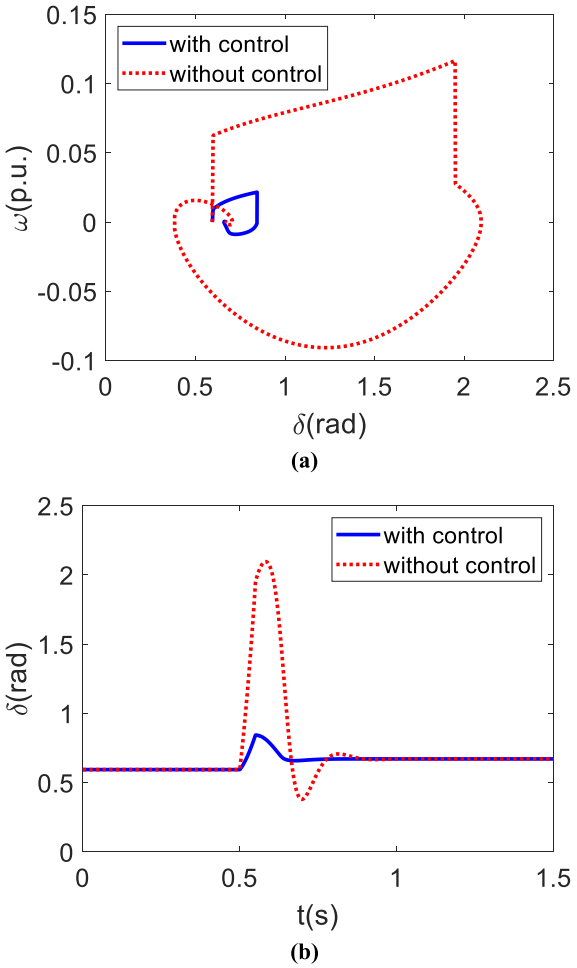

FIGURE 12. Comparison of the behaviors of transient stability without control (red dotted line) and with control (blue line) by clearing the fault 0.05s later after it occurs: (a) In the state space. (b) Waveform of δ in the time domain. Clearly with the control, the system performance in the transient increases.

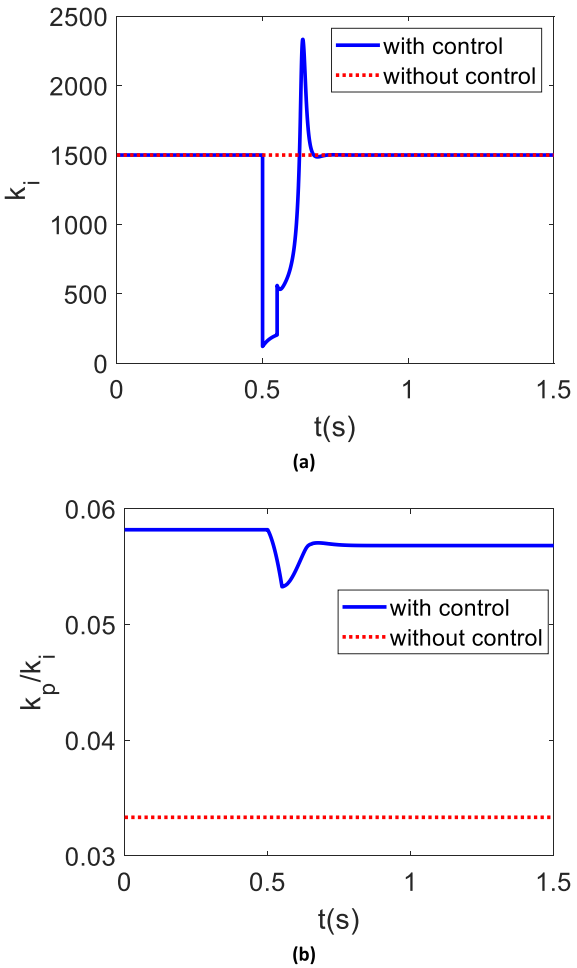

FIGURE 13. Comparison of k_p and $\frac{k_p}{k_i}$ without control (red dotted line) and with control (blue line) (a) k_p. (b) $\frac{k_p}{k_i}$.

smaller than 1.0 so that the $k_p > 0$. When $\cos\delta > 0, \frac{k_p}{k_i} > \frac{k_{p0}}{k_{i0}}$. When $\cos\delta < 0, \frac{k_p}{k_i} < \frac{k_{p0}}{k_{i0}}$. The equation corresponds to Tab. 3. The equivalent damping and inertia can be changed.

Then from (7) and (8), k_p is obtained as:

$$k_p = k_{p0}(1 - \frac{2}{\pi} arctan(\lambda_1 \omega \frac{d\omega}{dt}))(1 + \lambda_2 \cos\delta) \quad (9)$$

So the conditions of the system can be measured and the extra loops can be used to change the equivalent PI parameters of the PLL-VSC. The schematic of the improved adaptive control strategy is shown in Fig. 11. Different from the existing adaptive PI parameter methods in [30], the adaptive control strategy in this paper is designed from the perspective of equivalent inertia and damping, and the equivalent PI parameters can change as the state in the transient process.

However, the PI parameters should be constricted by considering the small-signal stability. On the basis of linear system theory, the following small-signal stability conditions are given [31]:

$$k_p < \frac{1}{i_{dref} L_g} \quad (10)$$

and

$$k_i < \frac{U_g \cos\delta_0}{i_{dref} L_g} k_p \quad (11)$$

where $L_g = \frac{X_g}{\omega_0}$ denotes the corresponding inductance of X_g. So the PI parameters should be subject to these control constraints.

C. VERIFICATION OF ADAPTIVE CONTROL METHOD

In the test, the system parameters for the PLL-VSC are chosen: $R_g = 0$pu, $X_g = 0.7$pu, $i_{dref} = 0.8$pu, $i_{qref} = -0.2$pu, $U_{gpre} = 1$pu, $U_{gduring} = 0.3$pu, $U_{gpost} = 0.9$pu, $k_{p0} = 50$, $k_{i0} = 1500$, $\lambda_1 = 1000$, $\lambda_2 = 0.9$. Note that under these conditions, the basin of attraction is a typical fish-like pattern, as in Fig.2. In the absence of control, the two parameters k_p and k_i do not change. With the control, the adaptive PI parameter control strategy is conducted by using

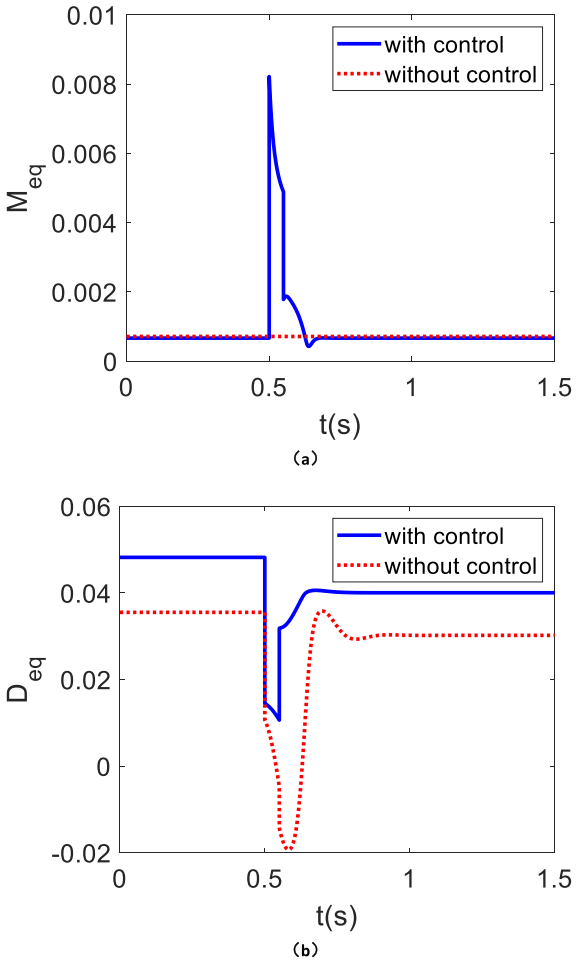

FIGURE 14. Comparison of equivalent inertia and damping without control (red dotted line) and with control (blue line) (a) M_{eq}. (b) D_{eq}.

the equivalent parameters in (7) and (9), which are guided according to the adaptive control strategy in Tab. 3.

Now compare the results without and with the adaptive PI parameter control strategy. First check the control strategy under the same clearing time after the during-fault process. When $t = 0.5s$, the fault occurs, clear the fault at $t = 0.55$s, showing the results in Fig. 12(a) for the state-space plot and Fig. 12(b) for the time-series plot. In this simulation, $U_{gpost} = 0.9$pu is smaller than $U_{gpre} = 1$pu, the angle δ doesn't converge to the its pre-fault value. If U_{gpost} is equal to U_{gpre}, the δ of the stable point will not change. The PLL-VSC is both stable, but the range of variation on the phase portrait becomes smaller after using the control, as shown in Fig. 12(a). Similarly the angle variation in the time domain in Fig. 12(b) also decreases after the control. All these show that the control method really improves the transient performance.

Next check the change of equivalent inertia and damping, the k_p and $\frac{k_p}{k_i}$ are shown in Fig. 13, after using the adaptive control strategy. Now the k_p and $\frac{k_p}{k_i}$ change in transient process. Similarly, the M_{eq} and D_{eq} are compared in Fig. 14, M_{eq} can change adaptively, and the D_{eq} become larger after using the adaptive control strategy, which enhances the transient stability of PLL-VSC. The CCA and CCT can be determined by the time domain simulation. The CCA has changed from 1.9865rad to 2.2672rad and the CCT from 0.0510s to 0.1924s. Both CCA and CCT increase after using the control, demonstrating that the adaptive PI parameter control strategy can enhance the transient stability.

IV. CONCLUSION

In conclusion, faced with the key challenges in the transient stability analysis of the PLL-VSC systems: the state-dependent nonlinear damping effect and two different types of basin of attraction for different system parameters [13], [18], we have developed a trajectory reversing method for the transient stability analysis and an adaptive control method for the transient stability enhancement. Our study finds that the trajectory reversing method is efficient and straightforward. The boundary of the stability region can be estimated more conveniently and systematically, compared with the Monte Carlo method and the time-domain simulation method. Compared with other methods, such as Lyapunov's direct method, energy function, and hyperplane method which highly rely on the local dynamical information of the controlling (or relevant) unstable equilibrium point, the TRM can discriminate two different types of basin of attraction well, where the closed-loop pattern is usually far away from the unstable equilibrium point. In this respect, the TRM is unique to solve the problem of two different types of basin of attraction by considering the state-dependent damping term. To the best knowledge of the authors, there is no any other method capable to deal with this problem. In addition, with this method, the EAC result which completely ignores the damping term can be easily compared.

For the second key contribution of this paper, directly from the physical understanding of the (generalized) swing equation for the vibration damping of mechanical systems in the transient process, an adaptive control strategy by varying the controller parameters (or equivalently the equivalent damping and inertia) on the basis of the system status is developed. Our study finds that this method is also efficient and straightforward. Only the information of signs of ω, $d\omega/dt$ and $\cos\delta$ are needed. It can attenuate the system disturbances quickly.

Therefore, we think that these two methods, although simple, can be valuable for the transient stability analysis and enhancement of the PLL-VSC systems. In the future, the trajectory reversing method and the adaptive PI controller should be examined in higher-order model.

REFERENCES

[1] M. Farrokhabadi et al., "Microgrid stability definitions, analysis, and examples," *IEEE Trans. Power Syst.*, vol. 35, no. 1, pp. 13–29, Jan. 2020.

[2] Z. Yang, R. Ma, S. Cheng, and M. Zhan, "Nonlinear modeling and analysis of grid-connected voltage-source converters under voltage dips," *IEEE J. Emerg. Sel. Topics Power Electron.*, vol. 8, no. 4, pp. 3281–3292, Dec. 2020.

[3] T. Qoria, F. Gruson, F. Colas, G. Denis, T. Prevost, and X. Guillaud, "Critical clearing time determination and enhancement of grid-forming converters embedding virtual impedance as current limitation algorithm," *IEEE J. Emerg. Sel. Topics Power Electron.*, vol. 8, no. 2, pp. 1050–1061, Jun. 2020.
[4] M. G. Taul, X. Wang, P. Davari, and F. Blaabjerg, "Systematic approach for transient stability evaluation of grid-tied converters during power system faults," in *Proc. IEEE Energy Convers. Congr. Expo. (ECCE)*, Baltimore, MD, USA, Sep. 2019, pp. 5191–5198.
[5] L. Guan and J. Yao, "Dynamic stability improvement scheme for dual-sequence PLLs in VSC based renewable energy generation system during asymmetrical LVRT," *Int. J. Electr. Power Energy Syst.*, vol. 145, Feb. 2023, Art. no. 108683.
[6] W. Tang, J. Hu, Y. Chang, and F. Liu, "Modeling of DFIG-based wind turbine for power system transient response analysis in rotor speed control timescale," *IEEE Trans. Power Syst.*, vol. 33, no. 6, pp. 6795–6805, Nov. 2018.
[7] Q. Peng, Y. Yang, T. Liu, and F. Blaabjerg, "Coordination of virtual inertia control and frequency damping in PV systems for optimal frequency support," *CPSS Trans. Power Electron. Appl.*, vol. 5, no. 4, pp. 305–316, Dec. 2020.
[8] X. Fu, J. Sun, M. Huang, Z. Tian, H. Yan, H. H. Iu, P. Hu, and X. Zha, "Large-signal stability of grid-forming and grid-following controls in voltage source converter: A comparative study," *IEEE Trans. Power Electron.*, vol. 36, no. 7, pp. 7832–7840, Jul. 2021.
[9] Q. Hu, L. Fu, F. Ma, F. Ji, and Y. Zhang, "Analogized synchronous-generator model of PLL-based VSC and transient synchronizing stability of converter dominated power system," *IEEE Trans. Sustain. Energy*, vol. 12, no. 2, pp. 1174–1185, Apr. 2021.
[10] Ö. Göksu, R. Teodorescu, C. L. Bak, F. Iov, and P. C. Kjær, "Instability of wind turbine converters during current injection to low voltage grid faults and PLL frequency based stability solution," *IEEE Trans. Power Syst.*, vol. 29, no. 4, pp. 1683–1691, Jul. 2014.
[11] H. Wu and X. Wang, "Transient stability impact of the phase-locked loop on grid-connected voltage source converters," in *Proc. Int. Power Electron. Conf. (IPEC-Niigata ECCE Asia)*, May 2018, pp. 2673–2680.
[12] J. Zhao, M. Huang, H. Yan, C. K. Tse, and X. Zha, "Nonlinear and transient stability analysis of phase-locked loops in grid-connected converters," *IEEE Trans. Power Electron.*, vol. 36, no. 1, pp. 1018–1029, Jan. 2021.
[13] R. Ma, J. Li, J. Kurths, S. Cheng, and M. Zhan, "Generalized swing equation and transient synchronous stability with PLL-based VSC," *IEEE Trans. Energy Convers.*, vol. 37, no. 2, pp. 1428–1441, Jun. 2022.
[14] Y. Tang, Z. Tian, X. Zha, X. Li, M. Huang, and J. Sun, "An improved equal area criterion for transient stability analysis of converter-based microgrid considering nonlinear damping effect," *IEEE Trans. Power Electron.*, vol. 37, no. 9, pp. 11272–11284, Sep. 2022.
[15] Y. Zhang, C. Zhang, and X. Cai, "Large-signal grid-synchronization stability analysis of PLL-based VSCs using Lyapunov's direct method," *IEEE Trans. Power Syst.*, vol. 37, no. 1, pp. 788–791, Jan. 2022.
[16] T. Wang, T. Ji, D. Jiao, Y. Li, and Z. Wang, "Transient synchronization stability analysis of PLL-based VSC using Lyapunov's direct method," *Int. J. Elect. Power Energy Syst.*, vol. 141, Oct. 2022, Art. no. 108135.
[17] C. Zhang, M. Molinas, Z. Li, and X. Cai, "Synchronizing stability analysis and region of attraction estimation of grid-feeding VSCs using sum-of-squares programming," *Frontiers Energy Res.*, vol. 8, no. 2020, p. 56, Apr. 2020.
[18] X. Wang, M. G. Taul, H. Wu, Y. Liao, F. Blaabjerg, and L. Harnefors, "Grid-synchronization stability of converter-based resources—An overview," *IEEE Open J. Ind. Appl.*, vol. 1, pp. 115–134, 2020.
[19] R. Ma, Y. Zhang, Z. Yang, J. Kurths, M. Zhan, and C. Lin, "Synchronization stability of power-grid-tied converters," *Chaos, Interdiscipl. J. Nonlinear Sci.*, vol. 33, no. 3, Mar. 2023, Art. no. 032102.
[20] R. Ma, Z. Yang, S. Cheng, and M. Zhan, "Sustained oscillations and bifurcations in three-phase voltage source converter tied to AC grid," *IET Renew. Power Gener.*, vol. 14, no. 18, pp. 3770–3781, Dec. 2020.
[21] Q. Hu, L. Fu, F. Ma, and F. Ji, "Large signal synchronizing instability of PLL-based VSC connected to weak AC grid," *IEEE Trans. Power Syst.*, vol. 34, no. 4, pp. 3220–3229, Jul. 2019.
[22] O. Abdoli, M. Gholipour, and R.-A. Hooshmand, "A novel method for synchronization stability enhancement of grid connected converters based on equal area criterion," *Int. J. Electr. Power Energy Syst.*, vol. 139, Jul. 2022, Art. no. 108062.
[23] H. A. Hamed, A. F. Abdou, E. H. E. Bayoumi, and E. E. EL-Kholy, "A fast recovery technique for grid-connected converters after short dips using a hybrid structure PLL," *IEEE Trans. Ind. Electron.*, vol. 65, no. 4, pp. 3056–3068, Apr. 2018.
[24] L. Hadjidemetriou, E. Kyriakides, and F. Blaabjerg, "An adaptive tuning mechanism for phase-locked loop algorithms for faster time performance of interconnected renewable energy sources," *IEEE Trans. Ind. Appl.*, vol. 51, no. 2, pp. 1792–1804, Mar. 2015.
[25] R. Genesio, M. Tartaglia, and A. Vicino, "On the estimation of asymptotic stability regions: State of the art and new proposals," *IEEE Trans. Autom. Control*, vol. AC-30, no. 8, pp. 747–755, Aug. 1985.
[26] A. Raza, Q. Huang, J. Li, O. Bamisile, M. Afzal, and G. Raza, "Adaptive drooping control scheme for VSC-MTDC system with multiple renewable energy sites based on variable droop constant," *Int. J. Electr. Power Energy Syst.*, vol. 144, Jan. 2023, Art. no. 108520.
[27] S. Tao, Z. Xin, L. Xiuzhi, M. Jianghua, and K. Deyang, "Research on alternating adaptive control strategy of moment of inertia and damping coefficient of VSG," in *Proc. Chin. Autom. Congr. (CAC)*, Hangzhou, China, Nov. 2019, pp. 180–185.
[28] X. He and H. Geng, "Transient stability of power systems integrated with inverter-based generation," *IEEE Trans. Power Syst.*, vol. 36, no. 1, pp. 553–556, Jan. 2021.
[29] X. He, H. Geng, J. Xi, and J. M. Guerrero, "Resynchronization analysis and improvement of grid-connected VSCs during grid faults," *IEEE J. Emerg. Sel. Topics Power Electron.*, vol. 9, no. 1, pp. 438–450, Feb. 2021.
[30] L. Soder, "Explaining power system operation to nonengineers," *IEEE Power Eng. Rev.*, vol. 22, no. 4, pp. 25–27, Apr. 2002.
[31] Y. Zhang, M. Han, and M. Zhan, "The concept and understanding of synchronous stability in power electronic-based power systems," *Energies*, vol. 16, no. 6, p. 2923, Mar. 2023.

DENGKE XU received the B.S. degree in electrical engineering from the Huazhong University of Science and Technology, Wuhan, China, in 2022, where he is currently pursuing the M.Eng. degree in electrical engineering with the State Key Laboratory of Advanced Electromagnetic Engineering and Technology, School of Electrical and Electronic Engineering.

His research interests include the stability and control of renewable energy dominated power systems, such as transient stability analysis and control strategy.

MENG ZHAN (Senior Member, IEEE) was born in Jingdezhen, Jiangxi, China, in 1974. He received the B.S. degree in physics and the Ph.D. degree in nonlinear physics from Beijing Normal University, Beijing, China, in 1996 and 2001, respectively.

He was a Postdoctoral Researcher with the National University of Singapore, Singapore, and the University of Toronto, ON, Canada, from 2001 and 2006. He joined the State Key Laboratory of Advanced Electromagnetic Engineering and Technology, School of Electrical and Electronic Engineering, Huazhong University of Science and Technology, Wuhan, China. He has long been engaged in the study of nonlinear dynamics theory of complex systems in multiple directions, such as coupled nonlinear systems, chaos synchronization and control, pattern formation, and complex network dynamics. He has authored or coauthored over 100 SCI articles in internationally peer-reviewed journals, which have been cited over 2600 times. His H-index is 29. His research interests include power system stability, power-electronics-based power system dynamics, and nonlinear analysis of power systems.